

Structural characterization of Am(III) and Pu(III)-DOTA complexes

M. Audras, L. Berthon, C. Berthon, D. Guillaumont, T. Dumas, M.-C. Illy, N. Martin, I. Zilbermann, Y. Moissev, Y. Ben Eliyahu, et al.

▶ **To cite this version:**

M. Audras, L. Berthon, C. Berthon, D. Guillaumont, T. Dumas, et al.. Structural characterization of Am(III) and Pu(III)-DOTA complexes. Inorganic Chemistry, 2017, 56 (20), pp.12248-12259. 10.1021/acs.inorgchem.7b01666 . cea-02421730

HAL Id: cea-02421730

https://cea.hal.science/cea-02421730

Submitted on 20 Dec 2019

HAL is a multi-disciplinary open access archive for the deposit and dissemination of scientific research documents, whether they are published or not. The documents may come from teaching and research institutions in France or abroad, or from public or private research centers.

L'archive ouverte pluridisciplinaire **HAL**, est destinée au dépôt et à la diffusion de documents scientifiques de niveau recherche, publiés ou non, émanant des établissements d'enseignement et de recherche français ou étrangers, des laboratoires publics ou privés.

Structural characterization of Am(III) and Pu(III)-DOTA complexes

Matthieu Audras[1], Laurence Berthon[1], Claude Berthon[1], Dominique Guillaumont[1], Thomas Dumas[1], Marie-Claire Illy[1], Nicolas Martin[1], Israel. Zilbermann[2], Yulia Moiseev[2], Yeshayahu.Ben-Eliyahu[2], S. Cammelli[3], Christophe. Hennig[4], Philippe Moisy[1].*

[1] CEA, Nuclear Energy Division, Research Department on Mining and fuel Recycling Processes, BP17171 F-30207 Bagnols-sur-Cèze, France

[2] Department of Chemistry, NRCN, IL-84190 Beer Sheva – Israel

[3] Synchrotron SOLEIL – L'Orme des Merisiers Saint-Aubin - BP 48 91192 Gif-sur-Yvette Cedex – France

[4] ESRF – 6 Rue Jules Horowitz, 38000 Grenoble – France

*: corresponding authors

KEYWORDS: DOTA, UV-visible spectrophotometry, NMR, EXAFS, DFT calculations, Americium, Plutonium, lanthanides

ABSTRACT: The complexation of DOTA ligand (1,4,7,10-tetrazacyclodecane-1,4,7,10-tetraacetic acid) with two trivalent actinides (Am^{3+} and Pu^{3+}) was investigated by UV-visible spectrophotometry, Nuclear Magnetic Resonance (NMR) spectroscopy and extended X-ray

absorption fine structure (EXAFS) in conjunction with computational methods. The complexation process of these two cations is similar to what has been previously observed with lanthanides(III) of similar ionic radius. The complexation takes places in different steps and ends up with the formation of a (1:1) complex $[(An(III)DOTA)(H_2O)]^-$ where the cation is bonded to the nitrogens of the ring, the four carboxylate arms and a water molecule is completing the coordination sphere. Nevertheless, the formation of An(III)-DOTA complexes is faster than the Ln(III)-DOTA systems of equivalent ionic radius. Furthermore, it is found that An-N distances are slightly shorter than Ln-N distances. Theoretical calculations have shown that the slightly higher affinity of DOTA toward Am over Nd is correlated with slightly enhanced Ligand-to-metal charge donation arising from oxygen and nitrogen atoms.

Introduction

The polyaminocarboxylate ligands form a promising family of f-element cations chelating agents. Due to the formation of strong complexes with actinides, these ligands could be used as hydrophilic complexants[1-4] in the actinide migration chemical process in geological environment and in actinide interaction with the human body in case of contamination. The specificity of the poly-amino-carboxylic acids is based on a very large coordination sphere involving carboxylate and nitrogen functions.[1, 5, 6] The complexes have coordination numbers ranging from 8 to 10 due to the ligand coordination and residual hydration. The stability of the Metal - poly amino carboxylate complexes increases with increasing the polydentate character of the ligands and with increasing the sum of the acid constant ($\sum$pKa) [1, 7-9]. Amongst the polyaminocarboxylate ligands, the DOTA macrocycle ligand (1,4,7,10-tetrazacyclodecane-1,4,7,10-tetraacetic acid, see

Figure 1) is described as a powerful chelating agent with the lanthanides(III)[4, 10-12] (log $\beta_1 \approx 25$ to 27). Complexes of lanthanides with DOTA have been the subject of many studies over the last years. This interest was enhanced upon discovery of the unusual chemical properties of the $[Ln(DOTA)]^-$ complexes as well as their successful practical applications. For instance, $[Gd(DOTA)]^-$ is used as contrast agent in magnetic resonance imaging[13, 14] and $[^{90}Y(DOTA)]^-$ has been suggested for cancer therapy when attached to monoclonal antibodies[15].

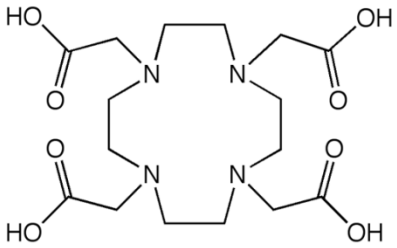


Figure 1. Developed formula of the DOTA molecule.

Solid state structures and coordination modes of the Ln-DOTA complexes are known for the whole lanthanide series[16, 17]. Eight coordination sites are occupied by the N and O donor atoms and the ninth site is occupied by a water molecule. From a general standpoint, the stability constant rises across the lanthanide series as the M-N length drops due to lanthanide contraction (reduced ionic radius and increasing effective charge). An X-ray absorption spectroscopy (EXAFS) study of the local structure around the Gd^{3+} ions in $[Gd(DOTA)(H_2O)]^-$ as crystal and in aqueous solutions shows that the gadolinium local environment is conserved up to 4.5 Å (in aqueous solution with pH 7 and is still so when the pH decreases to 1.5) [12, 18].

From a kinetic standpoint, many authors were surprised by the slowness of the formation of the thermodynamically stable complexes[19-24]. At room temperature and for stoichiometric or quasi stoichiometric ratios, it is necessary to wait several weeks and sometimes longer for the

formation equilibrium to stabilize[12, 25]. The reaction between Ln^{3+} ions and DOTA is slow and goes through the formation of intermediate species[12, 21, 25-27]. Different complexation mechanisms have been proposed in the literature[12, 19-25, 28-30] involving two or three distinct steps. This mechanism can be summed up as following. First, the cation gets bounded to the four oxygen atoms of the carboxylate groups. A stable intermediate, which is formed instantaneously, has been detected by spectrophotometry[20, 31], ^{1}H NMR[32], luminescence spectroscopy[33] and EXAFS[12]. It has been proposed that it is a diprotonated complex, $[Ln(H_2DOTA)(H_2O)_5]^+$, labelled C1, in which the Ln^{3+} ion is in an ”out-of-cage” position only coordinated by acetate groups and water molecules, while two nitrogen atoms of the ring are protonated.[12, 21, 22, 31, 33] This species then evolves: upon departure of the ring protons. The lanthanide ion moves into the cavity to form the $[Ln(DOTA)(H_2O)]^-$ species, labelled C2, in which the ion is bounded to the four nitrogen atoms, four carboxylate oxygen atoms and one water molecule.

The formation rates of the complexes $[Ln(DOTA)(H_2O)]^-$ were then found to be inversely proportional to the acidity of the solution[20, 31-33]. One can notice the ionic radius decrease along the series[34] goes along with an increase of the formation rate[21, 24, 25, 35], due to the raise of charge density of the cation. Furthermore, the final species present a significant flexibility since two conformers in solution were identified by NMR and modeling.[31-33, 36-43] For Ln-DOTA systems, the species switch from one conformer to another by inversion of the cyclene ring or by rotation of the ethylenic arms, resulting in Square AntiPrismatic (SAP) and Twisted Square AntiPrismatic (TSAP) geometries.[17, 31, 32, 36, 38, 44, 45] The distribution ratio of each conformer is mostly dependent on the ionic radius of the cation,[33] as a decrease of ionic radius will favor a preponderance of the SAP form, more compact. Moreover, for the smallest cations of the series,

several authors[33, 38] observed the departure of the capping water molecule, leading to octacoordinate species TSAP' and SAP'.

Although many publications exist regarding Ln-DOTA systems, very few works dealing with actinides(III) complexation by DOTA have been reported to the best of our knowledge.[46-49]. The trivalent actinides complexation by DOTA studies[47, 49] enabled the calculation of the stability constant of a (1:1) M-DOTA complex with Ac, Am and Cm (log β_1 = 19.6,[47] 23.95[49] and 24.02[49]/22.6[47] respectively). The formation constant for Americium(III) is slightly higher than for the similarly sized Nd(III) (log β_1 = 22.5,[50] 23.0[4]). A similar increase of stability constants from An(III) to Ln(III) complexes were reported with Diethylenetriaminepentaacetate (DTPA) ligands.[51, 52] The number of water molecules which are bound to Cm-DOTA complex were also determined by TRFLS (N_{wat} = 1.5±0.5)[49]. However, no structural data of the complexes in solution have been published so far. A recent study in gaseous phase by ESI-MS[48] showed differences of behavior between actinides(III)-DOTA and lanthanides(III)-DOTA. As a result the metal ligand bond nature, the Ln(III)-DOTA complexes are slightly more stable in gaseous phase than the An(III)-DOTA complexes whereas the complexation constants in solution are very close.[4, 9, 10, 47] It was suggested the slight discrepancy in gaseous phase could result from the enhancement of a difference in solution between the two series.

In this work, the complexation of two trivalent actinides (Am^{3+} and Pu^{3+}) was investigated in order to fill the gap in knowledge between trivalent actinides and lanthanides. The aims of this study are

1/ to investigate the An(III) complexation mechanism and kinetic and compare it to the Ln(III) behavior (formation of an intermediary species 'C1 complex' evolving towards a final complex 'C2 complex) thanks to the UV-visible spectrophotometry;

2/ to obtain structural information about the An(III)-DOTA species using complementary spectroscopic techniques (EXAFS, NMR) as well as theoretical calculation.

Experimental section

Due to the high radioactivity of both americium and plutonium, all the systems were manipulated in a glove box. All the experimentations were carried at room temperature (25°C).

Materials

Aqueous solutions were prepared using Milli-Q deionized (DI) water. Solutions containing nitric acid were prepared by dilution of a 1M standardized solution (Sigma-Aldrich).

The ligand solutions were then prepared by dissolution of the DOTA solid form (labelled H_4L, 98 %, Chematech) into DI water. The pH was measured using MColorpHast pH strips and was found to be about 3.5 ± 0.3 which is in accordance with the acid–base properties of the molecule (pKa_1 = 1.71, pKa_2 = 1.88, pKa_3 = 4.18, pKa_4 = 4.24, pKa_5 = 9.23, pKa_6 = 11.08.[53]

The plutonium(III) stock solution was prepared by reduction of purified plutonium(IV). For this, a plutonium(IV) stock solution was initially prepared by dissolution of freshly precipitated $Pu(OH)_4$ in 2 M hydrochloric acid. The reduction was then carried out by addition of a hundredfold molar excess of hydroxylamonium chloride (ClHA) under stirring. The full change in oxidation state was checked by spectrophotometry and the free acidity was evaluated by calculation at 1M.

The americium(III) stock solution was prepared by dissolution of americium oxide AmO_2 in 5M nitric acid. This solution was afterwards purified on an A-6-50Wx4 (200.00 mesh) resin column. The retrieved americium was then precipitated with 2M NaOH and dissolved again in 0.1M HNO_3. A potentiometric titration with 0.1 M NaOH determined the free acidity of the solution at 0.1M.

Methodology

Chemical conditions for the UV-Vis experiments

As already described in the literature[20, 31-33], the complexation by DOTA is strongly pH-dependent and triggers kinetic hindrances. On the other hand, actinides are sensitive to hydrolysis, which imposes one to work at high acidity. Hence, in order to bypass this double issue, it was decided to use the DOTA in great excess ($R_{L/M} \approx 100$). Presenting such an excess, the DOTA will act as a chemical buffer and will settle the pH of the solutions at about 3.5±0.3 at all times. Furthermore, the complexation will be likely to occur quite fast, hence preventing the cations from hydrolysis.

Moreover, this consequent excess of ligand will help accelerating the complexation kinetics. The time for reaching the thermodynamic equilibrium will be then reasonable (within two hours) with regard to the ligand radiolysis induced by the radioactive materials.

Spectrophotometry measurements

The M-DOTA solutions were prepared in Eppendorf flasks by direct pipetting and mixing of the stock solutions of Am(III) or Pu(III). In both cases, the ligand solution was introduced first, and then a calculated aliquot of the metal stock solution was added under vigorous stirring. The

obtained solutions then presented a hundred-fold ratio regarding the ligand/metal concentration ratio. The solutions were then immediately transferred into a 10mm quartz cuvette with a Teflon cap and monitored using a Varian Cary 50 UV-Vis spectrophotometer. As both of the metal ions were handled in a glove box, the data were collected using a homemade optic fiber bypass.

The spectra were recorded in the 450-700 nm range for the plutonium systems and in the 495-530 nm range for the americium system. The baselines for all the measurements were done using solutions containing DOTA in water at 3.5±0.3 and the spectrum of the free cation was recorded as well by appropriate dilution of the stock solutions.

Close successive measurements were done after contacting to ensure a proper follow-up of the different species formation. The first spectrum is recorded 2 minutes after mixing of the ligand and An(III) solutions (t_0 + 2min).

EXAFS measurements and data processing

Spectra for Am L_{III} edge were recorded at the Rossendorf beam line BM20 (ROBL) at ESRF (Grenoble, France). BM20 is equipped with a water-cooled double-crystal Si(111) monochromator. Higher harmonics were rejected by two collimating Pt coated mirrors. A 13-element Ge solid-state detector was used for data collection in the fluorescence mode. Energy calibration was carried out with a Zr foil (17998 eV at the absorption maximum).

EXAFS experiments at the Pu L_{III} edge were carried out on the MARS beamline at the SOLEIL synchrotron facility (ring operated at 2.75 GeV with 400 mA), dedicated to the study of radioactive materials. The optics of the beamline essentially consist of a water-cooled double-crystal monochromator, used to select the incident energy of the X-ray beam and for horizontal

focalization, and two large water-cooled reflecting mirrors that are used for high energy rejection (harmonic part) and vertical collimation and focalization.

All the measurements were recorded in double-layered solution cells (200 µL) specifically designed for radioactive samples at room temperature and filled up under argon atmosphere for the Pu(III) sample to avoid Pu(III) oxidation to Pu(IV).

Data processing was carried out using the Athena code[54]. The E_0 energy was set at the maximum of the absorption edge. The EXAFS signal was extracted by subtracting a linear pre-edge background and a combination of cubic spline functions for atomic absorption background and normalized by the Lengeler–Eisenberg procedure. Pseudo-radial distribution functions (PRDF) were obtained by Fourier transform in $k^3\chi(k)$ between 2.5 and 12 $Å^{-1}$.

Back-scattering amplitude and phase shift function are obtained from FEFF 8.2 calculation[55, 56] performed on the optimized DFT structures (see DFT section). All fitting operations are performed in R-space over individual radial distances (O, O_{water}, N, C) and Debye-Waller factors (σ^2) for every considered distances. Special care is taken to avoid overinterpretation by restricting σ^2 in a range on 10^{-2} to 10^{-3} $Å^2$ (exept for the water molecule)and by fixing coordination numbers and S_0^2 to 1. The R factor (%) and errors in distances are provided from ARTEMIS code[57].

RMN spectroscopy

^{1}H NMR experiments were performed with an Agilent DD2 400MHZ spectrometer equipped with a 5 mm OneNMR probe. Solutions containing actinides were placed in a double containment NMR tubes through dedicated glove boxes[58]. VnmrJ 4.2 software was

used for acquisition and data processing. A 10kHz proton spectral width was used for acquisitions and D_2O as lock diluent.

DFT calculations

The geometries of the DOTA complexes were optimized at the DFT level of theory with the Gaussian 09 program package. Aqueous solvation effects were taken into account by using an implicit solvation model where the solute is embedded inside a molecular-shape cavity surrounded by a dielectric medium. The Integral Equation Formalism Polarizable Continuum Model (IEFPCM) was used as implemented in Gaussian 09. The optimised structures were characterized as true minima through harmonic vibrational frequency analysis.

For metal ions, small-core relativistic effective core potentials (RECP) developed in the Stuttgart/Cologne group were used together with the accompanying basis set to describe the valence electron density.[59-62]The corresponding valence basis sets are the segmented (14s13p10d8f6g)/[10s9p5d4f3g] for Am, Pu and (14s13p10d8f6g)/[10s8p5d4f3g] for Nd. For other atoms, the 6-31+G(d,p) basis set was used. The M06L functional was employed[63]. The QTAIM analysis was carried out using AIMQB program package.[64]

Results

UV-visible Spectrophotometry

Spectrophotometry experiments were carried out on order to establish the An(III) complexation mechanism and kinetic. For the lanthanides analogs, the well-established complexation process goes through the formation of an intermediate species where the cation is

bonded to the carboxylates oxygens only (C1 complex) before ending up to the final complex (C2 complex) [12, 19-25, 28-30]. Thus, in this work, the first species formed just after addition of the cation to the ligand solution and the final species at thermodynamic equilibrium were labeled C1 and C2 respectively.

Figure 2 shows the kinetic follow-ups of the absorption spectrum for both Am(III) and Pu(III) – DOTA complexes. The absorption spectrum of Am(III) strongly depends on its chemical surrounding. The formation of Am–DOTA complexes results in a rise of the extinction coefficient value and to significant spectral changes compare to hydrated Am(III). In presence of DOTA, the Am(III) band of the aqua ion at 503 nm is instantaneously red shifted at 504.5 nm (t0+2min). Overtime, the absorption maximum is further red shifted by 7 nm at 510 nm. An isobestic point is found at 507 nm indicating the presence of two species in solution. The thermodynamic equilibrium reached after 100 minutes of reaction was considered when the absorption spectrum no longer evolved..

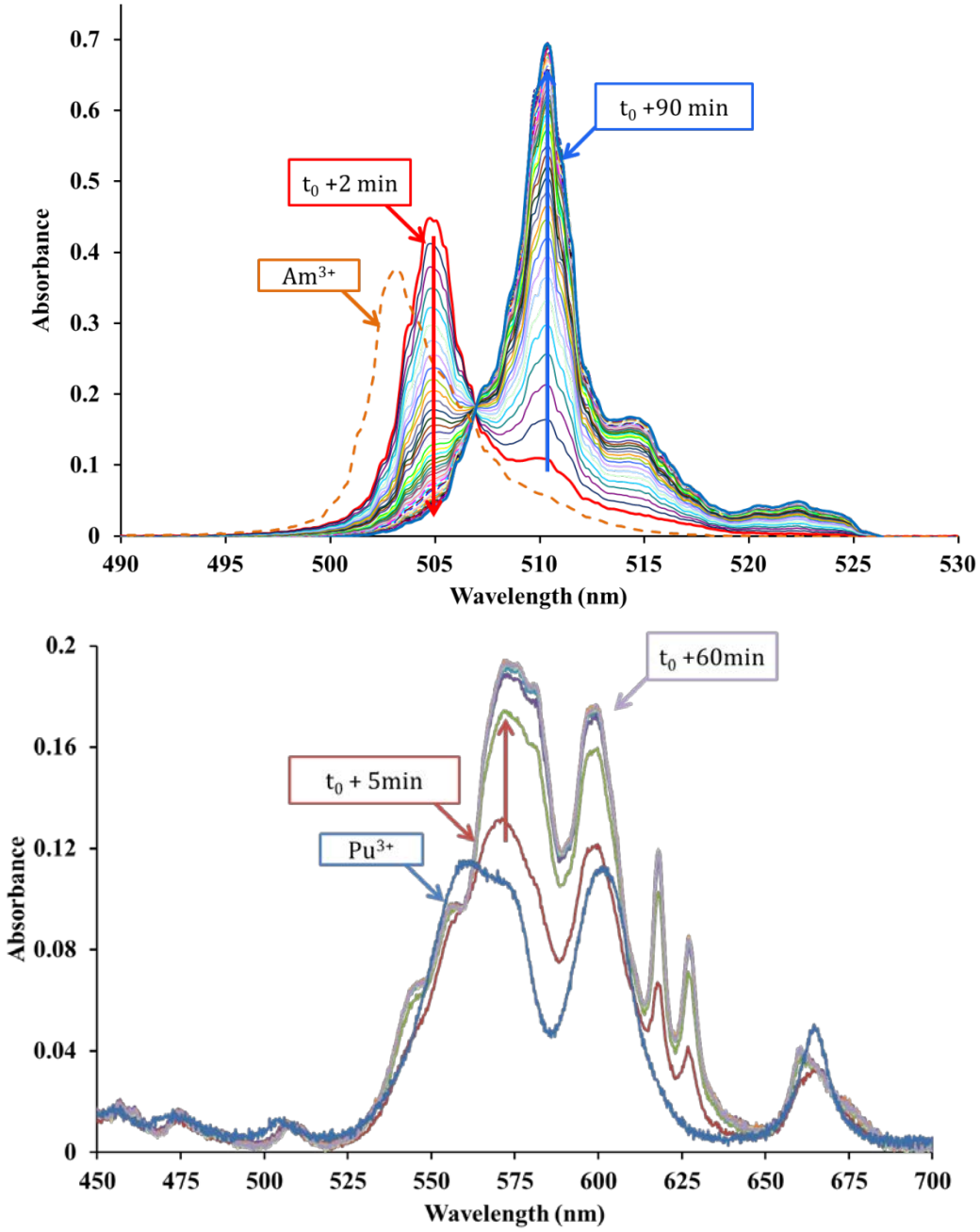


Figure 2. top: UV-Vis kinetic follow-up of the complexation of 10^{-3}M Am^{3+} by 0.1M DOTA in aqueous solution at pH = 3.5±0.3 and θ = 25°C. Dashed orange line: Am^{3+} 10^{-3}M in 0.1M HNO_3. t_0: addition of the metal solution to the ligand solution. Bottom: UV-Vis kinetic follow-up of the complexation of $3.6.10^{-3}$M Pu^{3+} by 0.2M DOTA in aqueous solution at pH = 3.5±0.3 and θ = 25°C. Blue line: 2.10^{-3}M Pu^{3+} in 1M HCl, 0.14M ClHA.

Upon plutonium addition to the DOTA solution, immediate (i.e. in less than a minute) spectral changes are observed, the absorption maximum of the band at 563 nm is red shifted at 573 and the band at 602 nm is blue shifted to 599 nm. While the main bands at 563 and 599 nm rise up, two additional peaks arise at 618 and 627 nm. As for Americium, the thermodynamic equilibrium was considered as reached when the absorption spectrum no longer evolves (after 60 min of reaction). It should be mentioned that the plutonium system is not stable overtime, after a few hours, the band intensities (572, 600, 518 and 627 nm) decreases while a band at 507 nm, identified as Pu(IV)-DOTA complex, concomitantly arise.

Thanks to these observations, we inferred the formation of the An(III)-DOTA species goes through the formation of an intermediate species before reaching the final thermodynamic equilibrium.

Kinetic aspects of the C1 → C2 transition

The apparent kinetic constants k_{app} corresponding to the formation of the final species (C2) from the intermediate species (C1) were determined. To determine k_{app}, the methodology consisted in assessing the proportion of each species (C1 and C2) with respect to time. The apparent kinetic constants of the C1 → C2 transition were then determined by direct deconvolution of the collected UV-Visible spectra. For this, the following assumptions were done:

at $t_0 + \varepsilon$, the complex is mainly under the C1 form only and a small part of the C2 form.

at $t_0 + \infty$, the complex is under the C2 form only (thermodynamic equilibrium).

No free cation are considered.

To determine the pure C1 UV-Vis spectrum for each system, the very first spectrum collected was used (t_0+2 min). The contribution of the C2 species (recorded at thermodynamic equilibrium) was gradually subtracted until its characteristic bands showed no more maxima at the corresponding wavelengths. The resulting spectra were then considered as the spectral signature of a pure C1 complex (see Figure S1 in Sup Info). A least square root deconvolution was applied to the experimental data with pure C1 and pure C2 as extremes, and the relative concentration of each species overtime are gathered Figure S2 in Sup Info. The variation of the logarithm of the concentration of the C1 complex versus time is plotted Figure 3 assuming a first-order kinetic law, with respect to the concentration of ligand. The slope of the straight line gives the apparent kinetic constant kapp of the C1→ C2 transition. The resulting values are $k_{appAmDOTA} = 0.75.10^{-3} \pm 0.10.10^{-3}$ s^{-1} and $k_{appPuDOTA} = 1.27.10^{-3} \pm 0.24.10^{-3}$ s^{-1}.

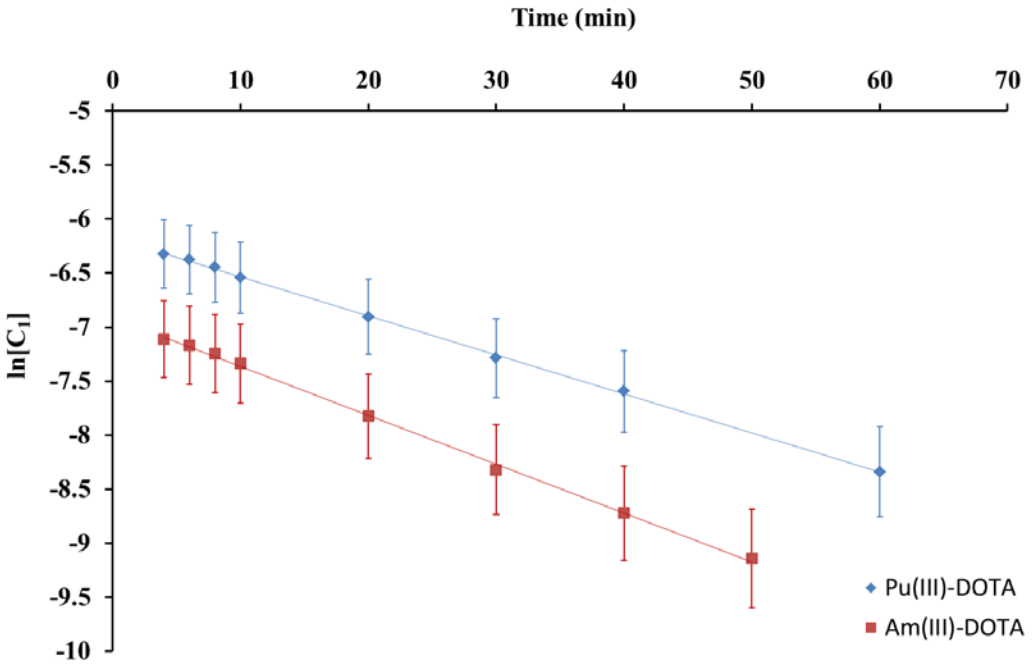


Figure 3: Evolution of ln[C1] upon complexation of americium(III) by DOTA (Composition : Am(III) 10^{-3} M, DOTA 0,2M in aqueous solution : [NO_3^-]= 0,07M, pH 3,5±0,3, ambiant temp.) and complexation of plutonium(III) by DOTA (Composition : Pu(III) $3{,}6.10^{-3}$ M, DOTA 0,2M in aqueous solution : [Cl-] = 0,66 M, [ClHA] = 0,36 M, pH 3,5±0,3 ambiant temp.).

The calculated kinetic constants for the C1 → C2 transition are of the same order of magnitude in the two systems, which is in accordance with Ln-DOTA systems[24, 35, 65] for consecutive elements with similar ionic radius ($ir_{Am(III)CN9}$ = 1,167 Å; $ir_{Pu(III)NC9}$ = 1,176 Å). To compare our results with some of the Ln-DOTA complexes, k_{app} value were extrapolated from the literature[21, 24-26, 35, 65] at pH 3.5 and reported Figure 4 for comparison with the measured actinide values. It clearly indicates that Pu(III)-DOTA and Am(III)-DOTA systems present a higher formation rate than the corresponding Ln(III)-DOTA systems of equivalent ionic radius.

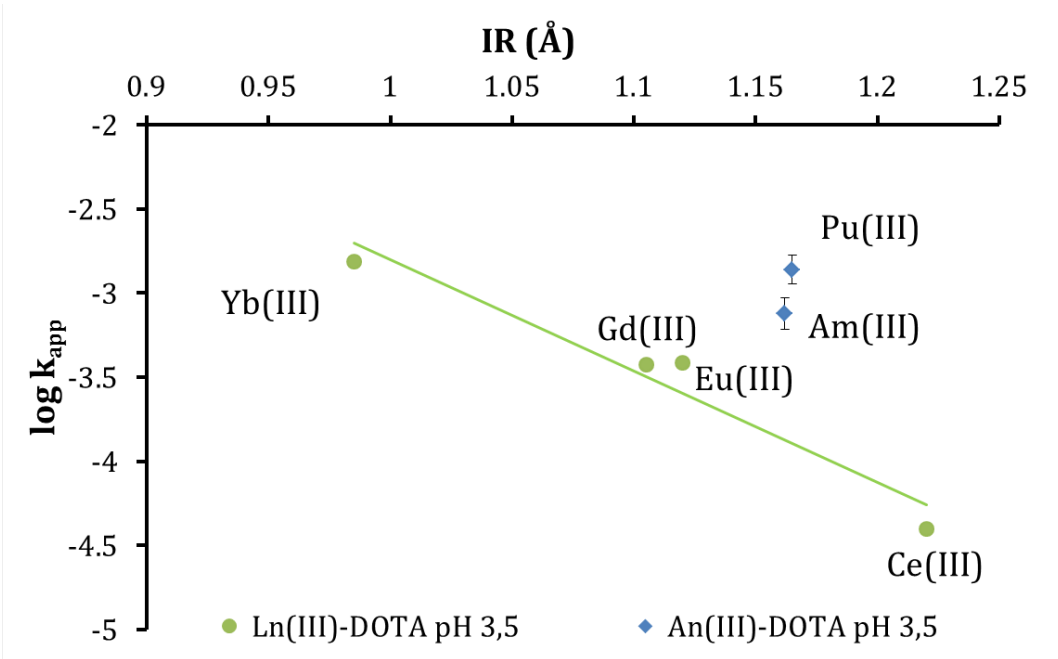


Figure 4: Variation of $\log k_{app}$ at pH 3,5 with respect to the ionic radius (CN= 9) of Ln(III)-DOTA and An(III)-DOTA complexes. For Ln(III)-DOTA the values are extrapolated from literature data [21, 24, 25, 35]

EXAFS

EXAFS experiments were performed to determine Pu(III)-DOTA and Am(III)-DOTA C2 complexes first coordination shells obtained at thermodynamic equilibrium. DFT calculations provided theoretical information on $[(PuDOTA)(H_2O)]^-$ and $[(AmDOTA)(H_2O)]^-$ that were used to model the EXAFS oscillations and will serve to compare distances. For the data analysis, no isomer in particular was considered, as a mixture of the two calculated species would have triggered too many parameters to fit. Moreover, the bond lengths of the calculated conformers differ by less than 0.05 Å in the first coordination sphere, which is higher than the accuracy provided by EXAFS. It would have then been irrelevant to take into account the two species. Figure 5 shows the k^3-weighted experimental, the Fourier Transform experimental and their least squares fitted EXAFS spectra for both Am(III)-DOTA and Pu(III)-DOTA systems. In both cases, the complex shapes of the k^3-weighted experimental EXAFS oscillations with significant shoulder at 5.1 $Å^{-1}$, and around 6.4 $Å^{-1}$ indicates destructive interferences in the first coordination shell from a complex geometry. It is confirmed on the FT's. As described by for lanthanides[12, 18] plutonium and americium experimental FT's consists in four main peaks. The two first peaks located at 1.5 Å < R+ϕ < 2.5 Å corresponds to single scattering (SS) path in the first coordination oxygen and nitrogen shell. The second double peak located at 2.5 Å < R+ϕ < 3.5 Å was assigned to cumulative effect of the 16 DOTA carbon. The first peak with a maximum at R+ϕ < 2 Å corresponding to shorter distances in the carboxylic group (An-O-C) while the second at R+ϕ > 2.7 Å corresponds to the DOTA ring. The last broad contribution at 3.5 Å < R+ϕ < 4.5 Å correspond to multiple scattering (MS) effects in the first and second coordination sphere and

from double and triple MS contributions from the quite linear An--C=O chain from carboxylate group.

The fitted distances to the metal ions are displayed in Table 1. In both cases, the experimental $[[(An(III)DOTA)(H_2O)]^-$ spectra is well fitted until $R+\phi = 3$ Å where MS effects (not considered in this fit) become predominant. However, the fit quality is good enough (R-Factor < 2.5 %) to assume the M^{3+} ion is surrounded by four carboxylate oxygen atoms at an average distance of 2.43 Å and 2.44 Å (for Am^{3+} and Pu^{3+} respectively), and four nitrogen atoms from the N-ring at an average distance of 2.67 Å and 2.68 Å. The first coordination sphere is completed by one water oxygen atom at 2.80 Å and 2.60 Å which must be considered with care for interpretation. The very high DWF obtained for the $An\text{-}O_{water}$ (0.023 $Å^{-1}$ and 0.014 $Å^{-1}$ respectively for the plutonium and americium) also observed for lanthanide[12] as well as the calculated error on bond length (0.10 Å and 0.07Å), indicate that the $An\text{-}O_{water}$ signal is weak in comparions to carboxylate and amino group and difficult to determine. The two carbon shell in second coordination sphere at 2.37 Å and 2.57 Å for Pu(III) and at 2.36 Å and 2.56 Å for Am(III) and four O shell (4.32 Å and 4.35 Å for plutonium and americium respectively) in the third coordination sphere were also considered to improve the fit quality.

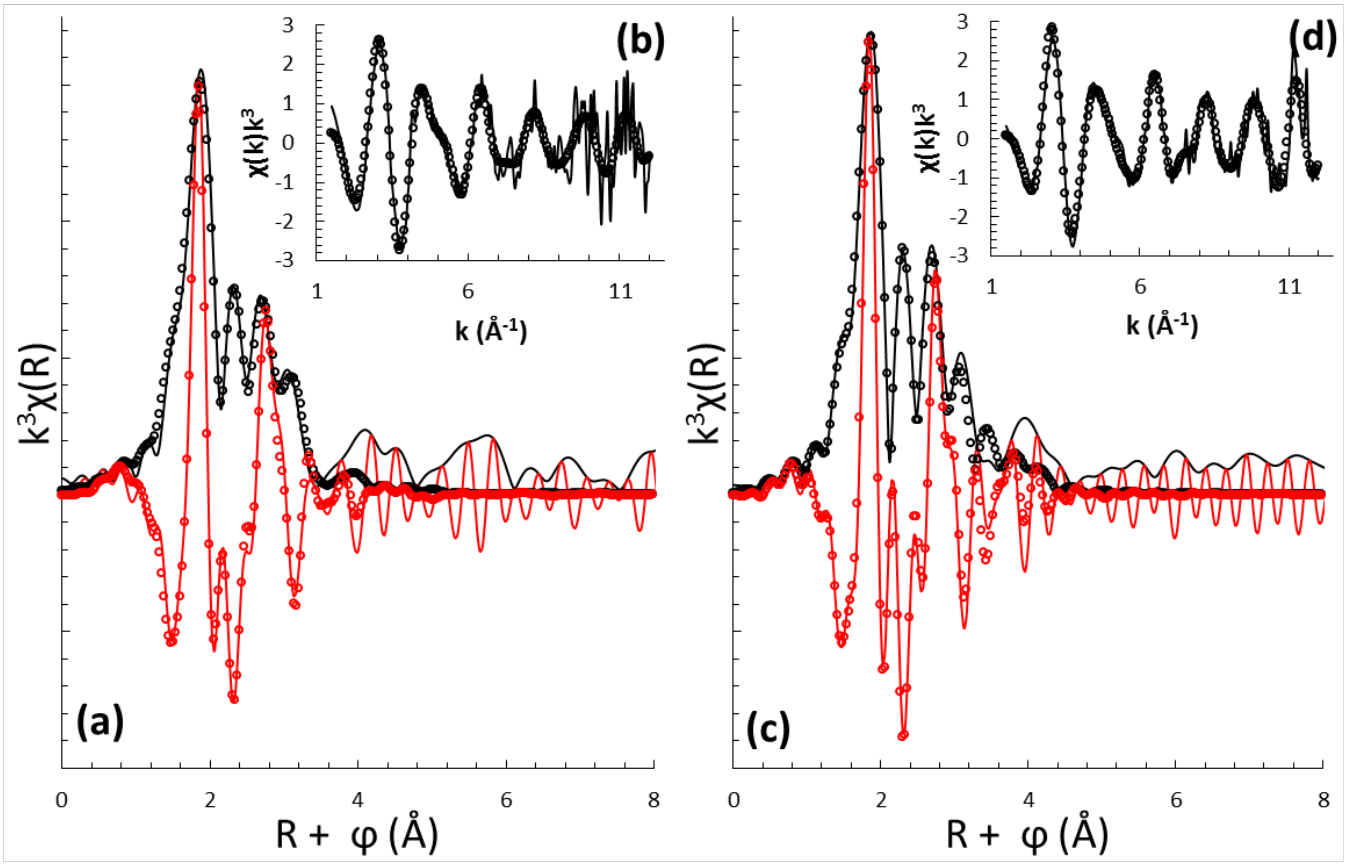


Figure 5: a: k^3-weighted experimental FT (black is magnitude and red is imaginary part) and fit (black and red open circle) spectra of the $[(PuDOTA)(H_2O]^-$ compound.

b: experimental (black) and fitted (open circle) k^3-weighted EXAFS spectra of the $[(PuDOTA)(H_2O]^-$ compound. Composition: Pu(III) 2.10^{-3} M, DOTA 0,2 M, NO_3^- 0,16 M, NHA 0,11 M, NH 0,024 M in water. pH 3±0,3

c: k^3-weighted experimental FT (black is magnitude and red is imaginary part) and fit (black and red open circle) spectra of the $[(AmDOTA)(H_2O]^-$ compound.

d: experimental (black) and fitted (open circle) k^3-weighted EXAFS spectra of the $[(PuDOTA)(H_2O]^-$ compound. Composition: Am(III) 10^{-3} M, DOTA 0,1 M, NO_3^-7,1.10^{-3} M in water. pH 3,5±0,3.

Table 1: EXAFS fit parameters for the $[PuDOTA(H_2O)]^-$ and $[AmDOTA(H_2O)]^-$ complexes $S_0^2 = 1$; $\Delta E_{k=0} = 6.07eV$. R-factor : 2.46%. N : Fixed Coordination number. Fiting range : 2 $Å^{-1}$ to 12 $Å^{-1}$.

	Pu-DOTA			Am-DOTA		
Diffusion path	**N**	**R (Å)**	**σ^2 (Å²)**	**N**	**R (Å)**	**σ2 (Å2)**
M – O	4	2.43±0.02	0.005	4	2.44±0,02	0.006
M – O_w	1	2.80±0.10	0.023	1	2.60±0,07	0.014
M – N	4	2.67±0.02	0.007	4	2.68±0,02	0.010
M – C_1	8	3.36±0.03	0.007	8	3.37±0,03	0.007
M – C_2	8	3.56±0.02	0.009	8	3.57±0,02	0.006
M-O_3	8	4.32±0.08	0.009	4	4.35±0,05	0.008

NMR

Proton spectral features of DOTA in water depend highly on the pH (see NMR supporting info, Figure S3).

^{1}H NMR of Pu^{III}-DOTA

^{1}H NMR spectra recorded on a DOTA in D_2O solution in presence of Pu(III) nitrate (with a ratio [DOTA]/[Pu(III)]=5) at pH 4. To circumvent the Pu^{III} oxidation into the DOTA complex, 5mg of Rongalite were added to the sample. (see NMR spectroscopy in supporting info, Figure S4 and S5). A set of broad peaks are observed between 1 and 6 ppm. Some of them are partially overlapped with water (4.6 ppm) and free DOTA ligand (3.7 and 3.2 ppm in ratio 1:2

respectively) signals. Considering the weak paramagnetic behavior of the Pu^{III} cation[66] the presence of about 100Hz large peaks is unexpected and may results from chemical exchange phenomena. This assumption is confirmed by changing temperature of NMR experiments (Figure 6). Temperature increase of the solution leads to a very broad peak at 46.5°C and at 84°C all proton signals belonging to the Pu(III) complex collapse into 2 peaks (Figure 6). They are at high field (3.1 and 2.9ppm) compared to those the free DOTA ligand and in a 2:1 ratio respectively. They are then assigned to the ethylenic groups of the ring and acetate arm protons respectively. At -4°C ^{1}H signals of the Pu(III)–DOTA complex spread out over a slightly larger spectral window and some sharp peaks appear. However the poor resolution achieved at this low temperature and the excess of free DOTA ligand precludes accurate assignment: the six ^{1}H peaks can be arbitrary drawn to two isomers (TSAP and SAP) of the Pu(III)-DOTA complex (Figure 7).

The Pu^{3+} ionic radius is similar to its $4f^5$ counterpart Pr^{3+} and chemical exchanges are also observed with the DOTA ligand[67]. It is noteworthy that Pr(III)-DOTA complex also exhibits only a few ^{1}H broad peaks at room temperature and two set of ^{1}H signals at low temperature in presence of deuterated MeOH at -4°C[68, 69] and up to -20°C (Figure 8). This phenomena stems from TSAP and SAP isomer exchange of the Pr(III)-DOTA complex but also from a water molecule exchange with the bulk. These exchanges also take place with the Pu(III) cation. However the narrow ^{1}H spectral feature of the Pu(III)-DOTA complex (about 6ppm) compared to those of the Pr(III) (spans from -60 to 45ppm) is explained by the weak paramagnetic behavior of the Pu(III) cation and prevents any further TSAP/SAP ^{1}H NMR assignments.

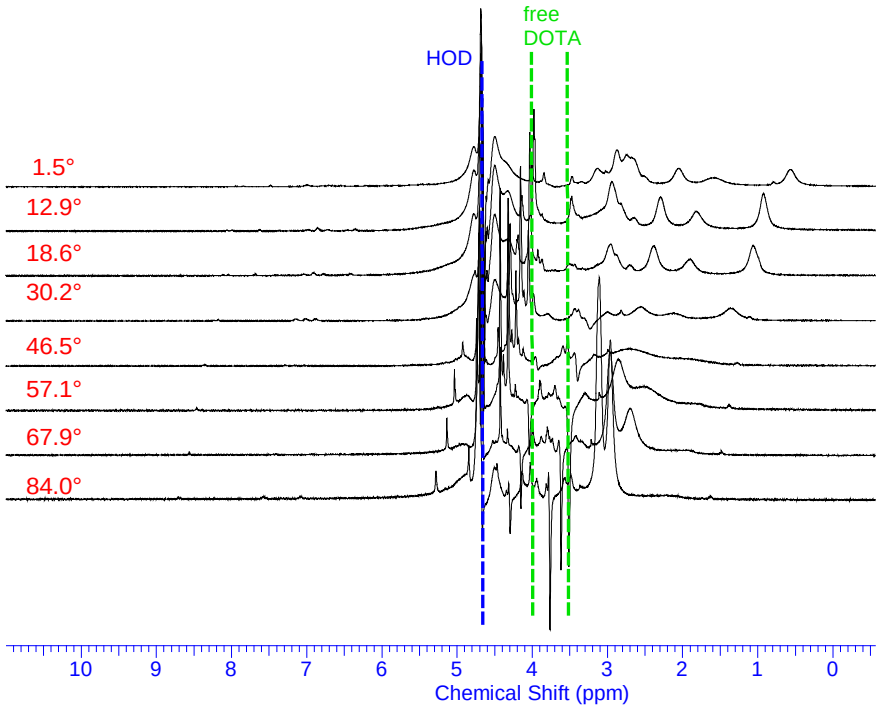


Figure 6: ^{1}H NMR spectra of 0.1M DOTA in D_2O with Pu(III) at different temperatures. [DOTA]/[Pu]=5 and pH=2. The pulse sequence used (WET1D) eliminated water and the free DOTA signals.

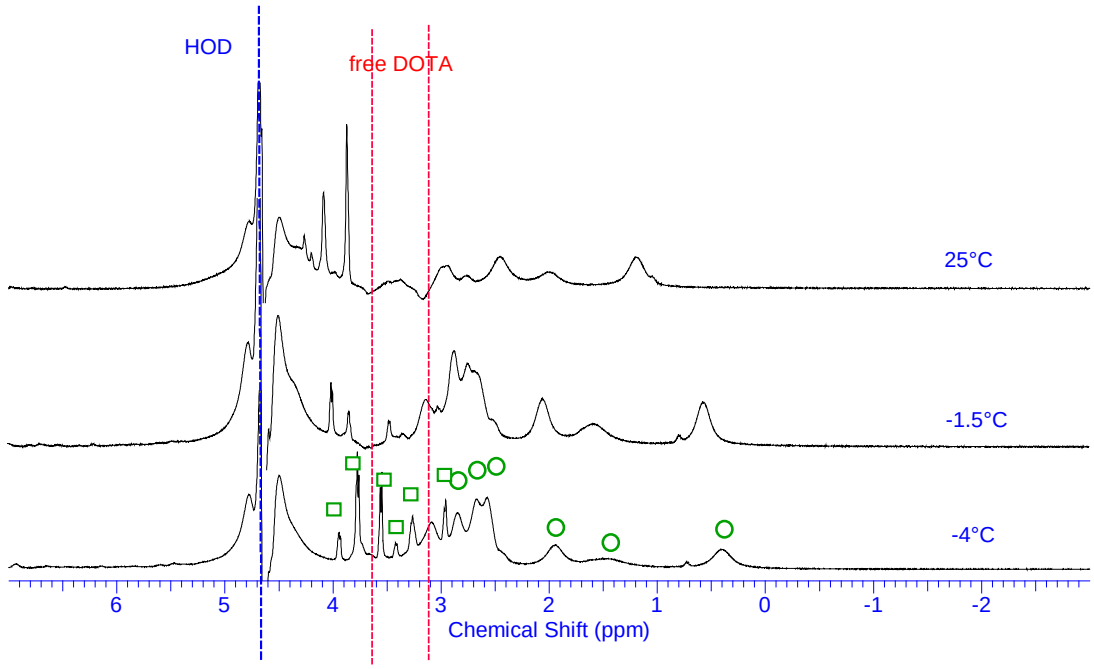


Figure 7: ^{1}H NMR spectra of 0.1M DOTA in D_2O with Pu(III) without (bottom one) and with water and free DOTA signal suppression (WET1D pulse sequence) to enhance resolution of the DOTA complex signals. Assignments of two isomer complexes are pointed with circle and square green tags at -4°C.

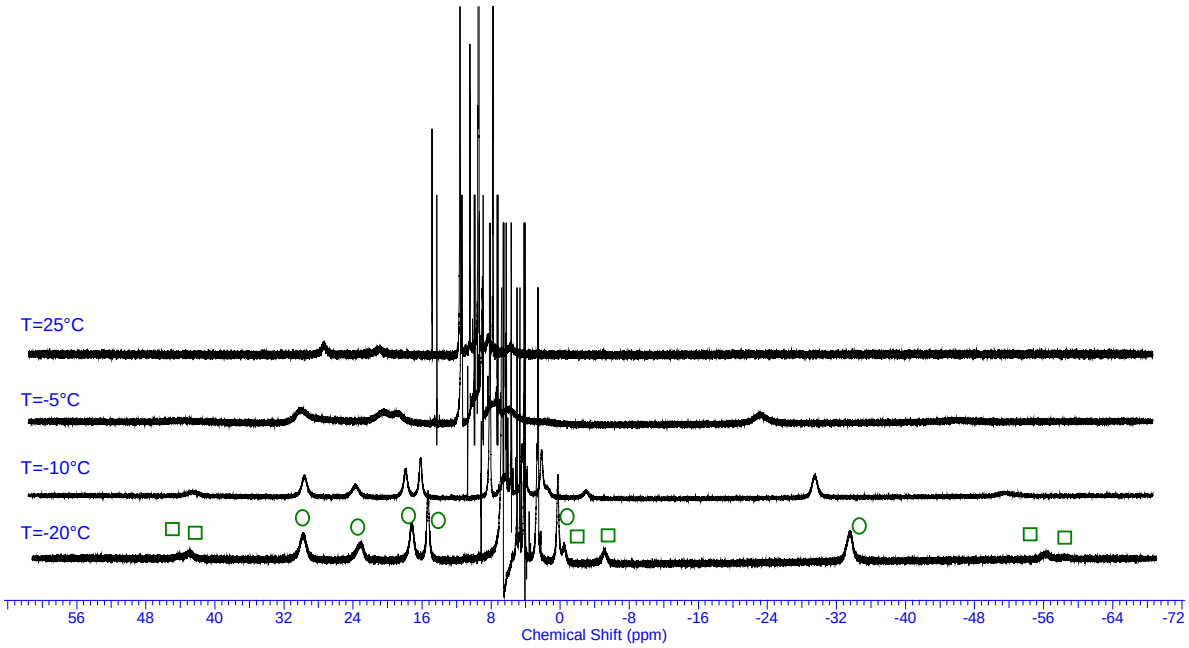


Figure 8: ^{1}H NMR spectra of Pr(III)-DOTA complex in D_2O/CD_3OD (50/50) at different temperatures. (WET1D pulse sequence). [DOTA]=14mM. Circle labels depict the TSAP isomer while square labels the SAP isomer.

^{1}H NMR of Am(III)-DOTA

^{1}H NMR spectra recorded on a 4mM DOTA solution with Am(III) nitrate ([DOTA]/[Am(III)]=2) set to pH 2.7 exhibit two set of peaks (Figure 9): two signals at 3.64 and 3.14ppm in a ratio 1:2 assigned to the free DOTA and the C1 Am(III)-DOTA complex and two other very broad peaks at 2.0 and 1.0ppm in a ratio 3:1 respectively assigned to the C2 Am(III)-DOTA complex. Indeed, integration ratios of the former decreases within 15hours of about 17% while the broad ones increase simultaneously of the same quantity due to the kinetic of the C1 → C2 transition. The evolution of the ^{1}H NMR spectra has already been reported for Ln(III)-DOTA complexes. [25]

Regarding Am(III)-DOTA isomers (TSAP/SAP) of the complex C2, very broad proton NMR signals we observed at room temperature. The weak paramagnetic property of the Am(III) cation does not account for this phenomemun, [66] but can be explained by a chemical exchange between the two (TSAP/SAP) isomers. Such dynamic process in DOTA complexes were observed for Nd(III) cations having ionic radius similar to Am(III). [33, 68] since peaks of both Nd(III)-DOTA isomers were assigned at -5°C on proton spectra and not at room temperature. It may also be possible that the water molecule exchange between the DOTA isomers and the bulk leads to broad signals as well.

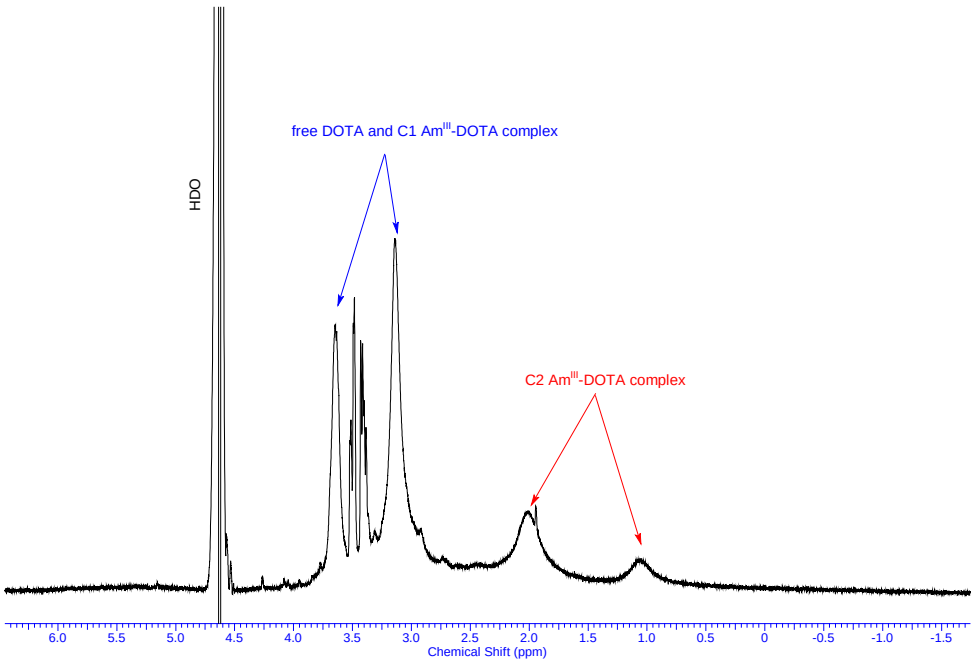


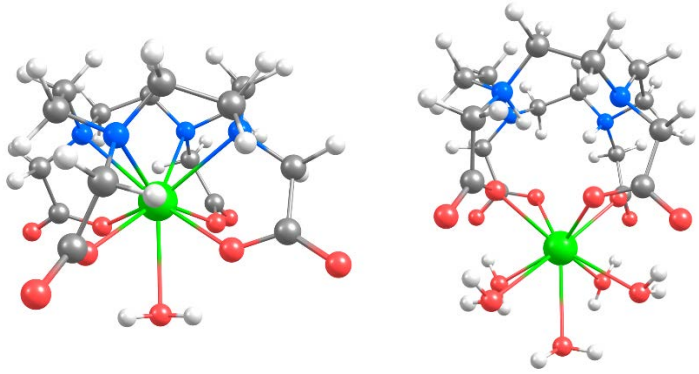
Figure 9: ^{1}H NMR spectrum of 0.1M DOTA in D_2O with Am^{III} nitrate. [DOTA]/[Am^{III}]=2 and pH=2.7.

From these data, it appears that Am(III) and Pu(III)-DOTA complexes have a behavior closed to those of the corresponding Ln(III)-DOTA complexes. At room temperature, a fast chemical exchange exists between the two (TSAP/SAP) isomers. In order to isolate and quantify each isomer, the exchanges have to be slowed down by decreasing the temperature. For that, the solvent has to be changed and this change of media will consequently lead to a behavior change of the TSAP/SAP isomers.

DFT Calculations

The geometries of the complexes and the metal-ligand bonds were investigated through quantum chemistry calculations. The calculations were performed on Pu(III), Am(III) and Nd(III). In the lanthanide series, Nd(III) was selected because its ionic radius is similar to both

actinides, it is slightly smaller than Am(III) and slightly larger than Pu(III)[70]. By comparing Metal-Ligand bonds within cations of similar sizes and coordination numbers, it is possible to avoid coordination structures changes along the cations and to minimize the error associated to solvent effects which are not very well described at such levels of calculations. The geometry of the complexes depicted in Figure 10 were optimized. $M(DOTA)(H_2O)^-$ complexes correspond to the final C2 structure with an encapsulated metal ion while $M(H_2DOTA)(H_2O)_5^+$ corresponds to the intermediate C1 structure in which the metal ion is in an "out-of-cage" position coordinated by four carboxylate oxygen atoms and five water molecules. In the later structure, the ligand has two hydrogen atoms located on two nitrogen atoms.



$M(DOTA)(H_2O)^-$ $M(H_2DOTA)(H_2O)_5^+$

Figure 10. Schematic representation of $M(DOTA)(H_2O)^-$ and $M(H_2DOTA)(H_2O)_5^+$ complexes. ●: C, ●: H, ●: O, ●: N, ●: M^{3+}.

The geometries of $M(DOTA)(H_2O)^-$ (C2) and $M(H_2DOTA)(H_2O)_5^+$ (C1) complexes were optimized in the gas phase and with a dielectric continuum model to describe solvent effect beyond the inner shell. For the final C2 complex, the calculations were done for the two SAP and TSAP diastereoisomers of Am(III) and Nd(III). The SAP isomer was found higher in energy for

both cations, by 9 kJ.mol^{-1} for Nd(III) and 13 kJ.mol^{-1} for Am(III), and was not further considered in the calculations. Metal-Oxygen and Metal-Nitrogen distances are collected in Table 2 for the TSAP isomers (C1 and C2) and in the DFT calculations section in supporting info for the SAP isomers. As determined from EXAFS, M-N distances calculated in solution are found shorter for Am(III), Pu(III) than for Nd(III) by 0.02-0.04 Å. It is interesting to note that this shortening is not reproduced in the calculations in the gas phase (Table 2) or for the SAP isomers in solution (See DFT calculations section in supporting info). This indicates that solvent effects beyond the inner coordination shell as well as the coordination chemistry around the metal ion have a significant effect on the metal-nitrogen bonds.

Table 2. Selected bond distances (Å) of M(DOTA)(H_2O)$^-$ (C2, TSAP isomer) and M(H_2DOTA)(H_2O)$_5^+$ (C1) in the gas phase and in aqueous solution calculated at the DFT/B3LYP level with experimental data, average values.

	M(DOTA)(H_2O)$^-$ C2			**M(H_2DOTA)(H_2O)$_5^-$ C1**	
	Gas	Sol.	Expr [a]	Gas	Sol.
Nd-O_{DOTA}	2.390	2.419	2.42	2.475	2.453
Am-O_{DOTA}	2.389	2.435	2.44	2.476	2.457
Pu-O_{DOTA}	2.385	2.439	2.43	2.479	2.474
Nd-N_{DOTA}	2.879	2.773	2.70	4.638	4.615
Am-N_{DOTA}	2.896	2.733	2.68	4.638	4.625
Pu-N_{DOTA}	2.933	2.753	2.67	4.631	4.643
Nd-O_{wat}	2.610	2.712	2.51	2.609	2.631
Am-O_{wat}	2.598	2.772	2.60	2.615	2.636
Pu-O_{wat}	2.623	2.768	2.80	2.632	2.629

[a] Nd values obtained from crystal data ([16]), Am and Pu values determined from EXAFS data in solution in this study

To compare metal-ligand bond strengths between actinides and lanthanides, binding energies were computed for the similarly sized Am(III) and Nd(III). To compare binding strength, the cation exchange reaction (1) was considered:

$Nd(H_2O)_9^{3+} + Am(DOTA)(H_2O)^- \rightarrow Am(H_2O)_9^{3+} + Nd(DOTA)(H_2O)^-$ (1)

To further examine to which extent nitrogen atoms favor actinide over lanthanide binding, cation exchange reaction (2) for "out-of-cage" complex C1 was also evaluated:

$Nd(H_2O)_9^{3+} + Am(H_2DOTA)(H_2O)_5^+ \rightarrow Am(H_2O)_9^{3+} + Nd(H_2DOTA)(H_2O)_5^+$ (2)

By using such exchange reactions instead of the complexation reaction, cancellation errors are expected to be maximized,[71]we avoid the hazardous energy calculation of the flexible free DOTA ligand with an unknown conformation and solvent effects are expected to be small for the reaction since it involves complexes of similar size in each side of the reaction. The binding energy differences for Nd → Am exchange reactions calculated in the gas phase and in the presence of a solvent model are given in Table 3. It is found that the binding strength is systematically stronger (more negative) for Am(III) than for Nd(III). As expected from the measured formation constants that differ by about one unit of $\log\beta_1$, small energy differences of a few $kJ.mol^{-1}$ are obtained for reaction (1) in term of both enthalpy and Gibbs free energy variations. Solution values for reaction (1) are only slightly more negative than gas phase values. The significant shortening of Am-N over Nd-N bond calculated in solution is only associated with a small enhancement of the DOTA binding strength compare to gas phase. The energy differences computed for reaction (2) (varying from -5 to -7 kJ.mol-1) confirm that carboxylate oxygen atoms favor Am complexation over Nd, as previously suggested from a DFT study on DTPA with Nd(III) and Am(III)[72]. Energy difference between reaction (1) and (2) is equal to 6

$kJ.mol^{-1}$ in solution indicating that nitrogen and carboxylate oxygen atoms play a similar role in the preferred complexation of actinides over lanthanides of similar sizes.

In order to rationalize the enhanced DOTA affinity for Am over Nd, the electronic structures of the complexes were analyzed from a Natural Population Analysis (NPA) and from a topological analysis employing the Quantum Theory of Atoms in Molecules (QTAIM). Metal-ligand bonds in trivalent actinides and lanthanides are predominantly ionic but differences between the two series are considered to be due to slightly larger covalency in actinides than lanthanides. In what follows, the hydrated ion $M(H_2O)_9^{3+}$, which is the starting point of the complexation reaction, is taken as the reference system. Rather than absolute properties calculated in the M-DOTA complexes, their deviations from the hydrated ions will be discussed, this is important to better represent the complexation reaction and to reduce any bias that may arise from the calculation methods. The metal partial charges derived from NPA and QTAIM analysis will be first discussed. Their values are given as the differences between the metal charge in the hydrated aqua ion and in the M-DOTA complexes inTable S2 (DFT calculations section in supporting info). Regardless of the metal cation and the calculation method (NPA or QTAIM), the metal charge is decreasing following the formation of the final C2 complex by about 0.2 e^-. The metal charges are also decreasing upon C1 formation indicating that nitrogen atoms as well as carboxylate oxygen atoms contribute similarly to DOTA-to-Metal charge donation and to the metal charge diminution. Returning to the Am/Nd comparison, the DOTA electron donation is slightly larger for Am than for Nd, the difference being larger from NPA than QTAIM. From NPA, the DOTA electron donation is 0.070 e^- larger in Am-DOTA than in Nd-DOTA in their C2 form and 0.035 e^- larger in the C1 complex. Therefore, N atoms and carboxylate O atoms contribute similarly to the enhanced DOTA charge donation toward Am

over Nd. Finally, there is a good match between binding energy and charge transfer. The enhanced DOTA affinity for Am over Nd, as determined from binding energies are associated with enhanced DOTA-to-Metal charge donation for Am over Nd. Calculated binding energies and metal charges for the C1 and C2 complexes point to the similar role played by nitrogen and carboxylate oxygen atoms in the preferred complexation of actinides over lanthanides of similar sizes.

Table 3. Free energy differences for the exchange reaction (1) and (2) (ΔH and ΔG^0 in kJ mol^{-1}, T=298 K) in the gas phase and in aqueous solution calculated at the DFT/B3LYP level

	Gas		Sol.	
	ΔH	ΔG	ΔH	ΔG
(1)	-8	-7	-11	-13
(2)	-6	-5	-7	-7

Table 4. Metal atomic partial charges variations upon formation of $M(DOTA)(H_2O)^-$ (C2) and $M(H_2DOTA)(H_2O)_5^-$ (C1) derived from QTAIM and NPA calculated in aqueous solution calculated at the DFT/B3LYP level

	$M(H_2O)_9^{3+} \rightarrow$ C2		$M(H_2O)_9^{3+} \rightarrow$ C1
	NPA	QTAIM	NPA
Nd	-0.162	-0.190	-0.090
Am	-0.232	-0.210	-0.125

The topological feature of the electron density was further analyzed from QTAIM. Such analysis can provide a powerful tool to quantify the degree of covalency in metal-ligand bonds and has been increasingly applied to probe bonding in trivalent actinides and lanthanides complexes[72-78]. This method consists in analyzing the gradient of the electron density $\nabla\rho$ to

characterize the topological features.[79] Chemical bonds are characterized by the presence of Bond Critical points (BCP) between atomic pairs. For the DOTA complexes, the QTAIM analysis found BCPs between the metal cation and each coordinated nitrogen and oxygen atoms, confirming the presence of M-O and M-N chemical bonds. The most important topological parameters (the density ρ, the Laplacian $\nabla^2\rho$, and the total energy density H(r) at the BCPs) are collected in Table S3 in DFT calcultations section in supporting info. Their values are characteristic of weak dative bonds and are of the same order of magnitude than those reported in actinide and lanthanides complexes with DTPA but also with aromatic nitrogen ligands.[80] If we turn to Am/Nd comparison, the magnitude of the BCP data in the C2 complexes are indicative of slightly more covalent Am-DOTA in comparison with Nd-DOTA (values of ρ and $\nabla^2\rho$ are larger while H are more negative). However, BCP data calculated in the hydrated ions are also indicative of slightly more covalent Am-O bonds and if we compare the variation of the metrics between M-O bonds in $M(H_2O)_9^{3+}$ and M-O and M-N bonds in $M(DOTA)(H_2O)^-$, the differences are getting very small and it is difficult to establish enhanced covalency in americium bonds from such analysis. As suggested in a recent study, atomic charges seem to be a better indicator of actinide bond energies.[81]

As a summary, we have found small differences between Am and Nd, however the differences are very consistent with experimental data; the DOTA binding strength is slightly larger for Am than for Nd, as measured from formation constants. The slightly higher affinity of DOTA toward Am over Nd is correlated with slightly enhanced Ligand-to-Metal charge donation. According to the calculations performed on the two C1 and C2 structures, all the DOTA donor atoms contribute equally to the enhanced affinity toward Am.

Discussion

From the UV-visible spectrophotometry observations, one can state the formation of the An(III)-DOTA species goes through the formation of an intermediate species before reaching the final thermodynamic equilibrium. Indeed, the slight change in spectra shape after a short time period is characteristic of a coordination sphere modification. This result means an intermediate species C1 instantaneously forms upon addition of the DOTA ligand. As for the lanthanides[4, 10, 12, 16] the actinide would be therefore bonded to four carboxylate oxygens, while the coordination sphere is completed by water molecules[4, 16, 18].This species would slowly evolves into the final species (C2) by intramolecular rearrangement: the metallic cation gets inside the cage formed by the macrocycle, while the water molecules leave the coordination sphere. This mechanism was partly confirmed by EXAFS and NMR spectroscopy that concomitantly were used to probe the structure of the C2 complex analogous to lanthanides.

The comparison of the apparent kinetic constants of the C1 → C2 transition between the Ln(III)-DOTA and An(III)-DOTA systems indicates that the C2 species present a higher formation rate for the An(III)-DOTA species than the Ln(III)-DOTA species of equivalent ionic radius (Figure 4).

Furthermore, the structural probing by EXAFS confirmed the two systems end up with the formation of a (1:1) complex $[(An(III)DOTA)(H_2O)]^-$ where the cation is bonded to the nitrogens of the ring, the four carboxylate arms and a water molecule is completing the coordination sphere (C2 complex), as what has been previously observed with Ln(III)-DOTA systems[12, 18]. Calculated distances in $[(An(III)DOTA)(H_2O)]^-$ in solution are in good agreement with

experimental distances. Calculated and measured M-O(DOTA) distances differ by less than 0.01 Å, while M-N distances are systematically longer by 0.07 Å but the metal-nitrogen shortening from Nd(III) to Am(III) is very well reproduced in the calculations. Only the M-O_{water} distance is poorly reproduced in the calculations, additional explicit water molecules in the model could improve the description of this bond. More importantly, the evolution of metal-DOTA bonds with the shortening of M-N bonds from Nd(III) to Am(III) and Pu(III is very well reproduced in the calculations.

In order to compare the An(III)-DOTA bond lengths to those of the lanthanide series, we used the available crystallographic data for Ln-DOTA systems. Indeed, Benazeth et al. [18] and Moreau et al. [12] proved the bond lengths obtained by crystallographic measurements (solid form) and EXAFS (complex in solution) do not differ. The only difference observed lies on the water molecule with a longer M-Ow distance in solution, which may due to the agitation of the water molecule in solution. The available data[12, 16] for the M-O and the M-N distances as well as the results of the present work are gathered in Figure 11.

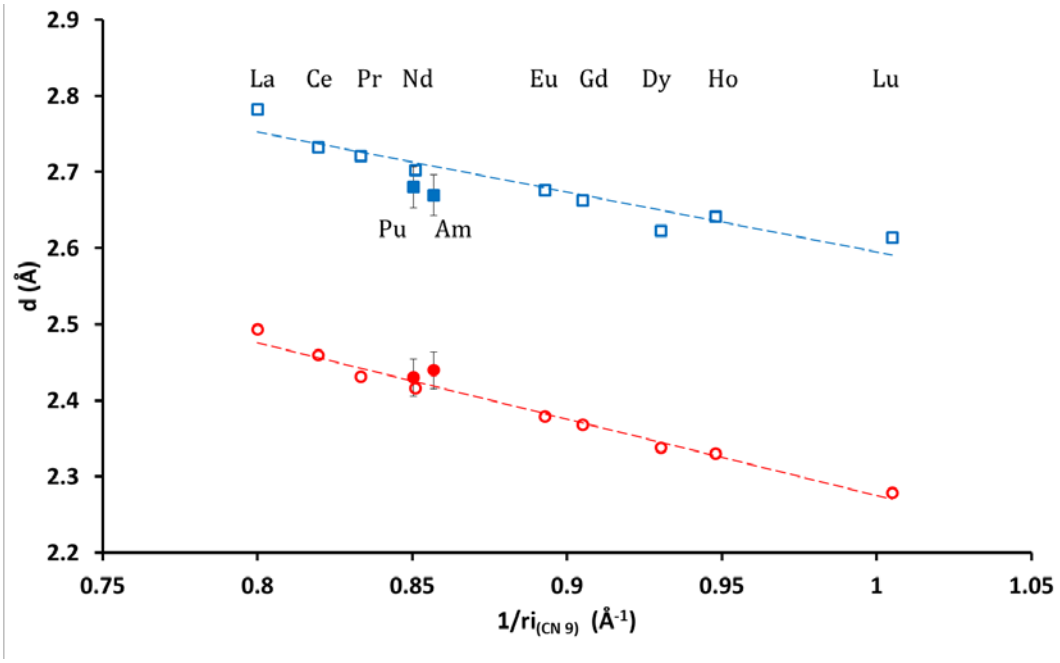


Figure 11: Plot of average M-N and M-O distances vs. 1/ir of lanthanides, Pu^{3+} and Am^{3+} with CN = 9. Lanthanide data were taken from [12, 16] and the ionic radii from ref[34, 82] and [83]. Empty circle: Ln-O distances ; full circle An-O distances ; empty square: Ln-N distances and full square An-N distances.

For the same ionic radius, M-O bond lengths are quite similar for actinide complexes as for lanthanide complexes. However, the M-N distances are slightly shorter for the complexes actinides complexes than for the lanthanides complexes of equivalent ionic radius[12, 16]. In effect, the M-N distance of the Am(III)-DOTA complex (2.67 ± 0.02 Å) is lower than that of the Nd(III)-DOTA (2.70 Å) complex, of equivalent ionic radius [83, 84]. The same observations can be made between the Pu (III)-DOTA complexes and the Pr(III)-DOTA complexes.[83, 84]

Otherwise, theoretical calculation have been shown that the binding strength is systematically stronger for Am(III) than for Nd(III) which is consistent with the measured formation constants. Moreover, it has been found that the Metal-Ligand bond in trivalent actinides an lanthanides are predominantly ionic but differences between the two series are considered to be due to slightly larger covalency in actinides than lanthanides.

Regarding the apparent kinetic constants of the C1 → C2 transition, the slow step in the complexation is the deprotonation of the nitrogen atoms accompanied by the entrance of the cation in the cage formed by the macrocycle leading to the formation of M-N connections[12, 85]. Calculation have been shown that the carboxylate oxygen atom favor Am complexation over Nd. Therefore, the faster kinetics of complexation of An (III) could be explained by the fact that the latter would faster form bonds with the nitrogens of cycle than the Ln(III). It would thus lead to a

faster formation of the C2 complex. Studies of trivalent cations of the beginning and the end of the actinide series could come to confirm these initial findings.

Conclusions

The DOTA ligand has been studied with respect to complexation of two trivalent actinides in aqueous solution: Am^{3+} and Pu^{3+}. The complexation process of these two cations is similar to what has been previously observed with lanthanides(III) of similar ionic radius. The complexation takes places in different steps and ends up with the formation of a (1:1) complex where the metallic cation is inside the cage formed by the macrocycle. The apparent kinetic constant of the transition between the intermediary species C1 and the final species C2 has been calculated thanks to UV-Visible spectrophotometry.

Furthermore, the structural probing by EXAFS confirmed the two systems end up with the formation of a (1:1) complex $[(An(III)DOTA)(H_2O)]^-$ where the cation is bonded to the nitrogens of the ring, the four carboxylate arms and a water molecule is completing the coordination sphere (C2 complex), as what has been previously observed with Ln(III)-DOTA. The formation of An(III)-DOTA complexes is faster than the Ln(III)-DOTA systems of equivalent ionic radius. From the EXAFS analysis in solution, it is found that An-N distances are slightly shorter than Ln-N distances. Theoretical calculations have shown that the DOTA binding strength are slightly larger for Am than for Nd (of similar ionic radius). Moreover, the slightly higher affinity of DOTA toward Am over Nd is correlated with slightly enhanced Ligand-to-metal charge donation arising from oxygen and nitrogen atoms.

Acknowledgements

The authors would like to thank the SOLEIL and ESRF synchrotrons during the EXAFS experiments.

Corresponding Author

laurence.berthon@cea.fr

REFERENCES

1. G. R. Choppin, P. Thakur and J. N. Mathur, *Coordination Chemistry Reviews*, **2006**, 250, 936-947.
2. S. Leguay, T. Vercouter, S. Topin, J. Aupiais, D. Guillaumont, M. Miguirditchian, P. Moisy and C. Le Naour, *Inorg. Chem.*, **2012**, 51, 12638-12649.
3. M. A. Brown, A. Paulenova and A. V. Gelis, *Inorg. Chem.*, **2012**, 51, 7741-7748.
4. W. P. Cacheris, S. K. Nickle and A. D. Sherry, *Inorg. Chem.*, **1987**, 26, 958-960.
5. W. Hummel, I. Puigdomenech, L. Rao and O. Tochiyama, *Comptes Rendus Chimie*, **2007**, 10, 948-958.
6. M. Meyer, R. Burgat, S. Faure, B. Batifol, J.-C. Hubinois, H. Chollet and R. Guilard, *Comptes Rendus Chimie*, **2007**, 10, 929-947.
7. T. F. Gritmon, M. P. Goedken and G. R. Choppin, *Journal of Inorganic & Nuclear Chemistry*, **1977**, 39, 2021-2023.
8. J. N. Mathur, P. Thakur, C. J. Dodge, A. J. Francis and G. R. Choppin, *Inorg. Chem.*, **2006**, 45, 8026-8035.
9. P. Thakur, P. N. Pathak, T. Gedris and G. R. Choppin, *J. Solut. Chem.*, **2009**, 38, 265-287.
10. M. F. Loncin, J. F. Desreux and E. Merciny, *Inorg. Chem.*, **1986**, 25, 2646-2648.
11. K. Kumar, T. Z. Jin, X. Y. Wang, J. F. Desreux and M. F. Tweedle, *Inorg. Chem.*, **1994**, 33, 3823-3829.
12. J. Moreau, E. Guillon, J.-C. Pierrard, J. Rimbault, M. Port and M. Aplincourt, *Chemistry – A European Journal*, **2004**, 10, 5218-5232.
13. R. B. Lauffer, *Chem. Rev.*, **1987**, 87, 901-927.
14. N. A. Viola, R. S. Rarig, W. Ouellette and R. P. Doyle, *Polyhedron*, **2006**, 25, 3457-3462.
15. D. Parker, *Chemical Society Reviews*, **1990**, 19, 271-291.
16. N. Viola-Villegas and R. P. Doyle, *Coordination Chemistry Reviews*, **2009**, 253, 1906-1925.
17. M. Meyer, V. Dahaoui-Gindrey, C. Lecomte and L. Guilard, *Coordination Chemistry Reviews*, **1998**, 178, 1313-1405.
18. S. Benazeth, J. Purans, M. C. Chalbot, M. K. Nguyen-van-Duong, L. Nicolas, F. Keller and A. Gaudemer, *Inorg. Chem.*, **1998**, 37, 3667-3674.
19. A. Bianchi, L. Calabi, C. Giorgi, P. Losi, P. Mariani, P. Paoli, P. Rossi, B. Valtancoli and M. Virtuani, *Journal of the Chemical Society-Dalton Transactions*, **2000**, 697-705.

20. K. Kumar and M. F. Tweedle, *Inorg. Chem.*, **1993**, 32, 4193-4199.
21. E. Brucher, G. Laurenczy and Z. Makra, *Inorganica Chimica Acta*, **1987**, 139, 141-142.
22. E. Brucher and A. D. Sherry, *Inorg. Chem.*, **1990**, 29, 1555-1559.
23. S. P. Kasprzyk and R. G. Wilkins, *Inorg. Chem.*, **1982**, 21, 3349-3352.
24. X. Y. Wang, T. Z. Jin, V. Comblin, A. Lopezmut, E. Merciny and J. F. Desreux, *Inorg. Chem.*, **1992**, 31, 1095-1099.
25. E. Toth, E. Brucher, I. Lazar and I. Toth, *Inorg. Chem.*, **1994**, 33, 4070-4076.
26. L. Burai, I. Fabian, R. Kiraly, E. Szilagyi and E. Brucher, *Journal of the Chemical Society-Dalton Transactions*, **1998**, 243-248.
27. X. Y. Wang, T. Z. Jin, V. Comblin, A. Lopezmut, E. Merciny and J. F. Desreux, *Inorg. Chem.*, **1992**, 31, 1095-1099.
28. E. Szilagyi, E. Toth, Z. Kovacs, J. Platzek, B. Raduchel and E. Brucher, *Inorganica Chimica Acta*, **2000**, 298, 226-234.
29. A. Bianchi, L. Calabi, L. Ferrini, P. Losi, F. Uggeri and B. Valtancoli, *Inorganica Chimica Acta*, **1996**, 249, 13-15.
30. E. T. Clarke and A. E. Martell, *Inorganica Chimica Acta*, **1991**, 190, 37-46.
31. S. Hoeft and K. Roth, *Chemische Berichte*, **1993**, 126, 869-873.
32. J. F. Desreux, *Inorg. Chem.*, **1980**, 19, 1319-1324.
33. S. Aime, M. Botta, M. Fasano, M. P. M. Marques, C. Geraldes, D. Pubanz and A. E. Merbach, *Inorg. Chem.*, **1997**, 36, 2059-2068.
34. R. D. Shannon, *Acta Crystallogr. A, Cryst. Phys. Diffr. Theor. Gen. Crystallogr.*, **1976**, A32, 751-767.
35. S. L. Wu and W. D. Horrocks, *Inorg. Chem.*, **1995**, 34, 3724-3732.
36. S. Aime, M. Botta and G. Ermondi, *Inorg. Chem.*, **1992**, 31, 4291-4299.
37. F. Benetollo, G. Bombieri, L. Calabi, S. Aime and M. Botta, *Inorg. Chem.*, **2003**, 42, 148-157.
38. F. Mayer, C. Platas-Iglesias, L. Helm, J. A. Peters and K. Djanashvili, *Inorg. Chem.*, **2011**, 51, 170-178.
39. V. Jacques and J. F. Desreux, *Inorg. Chem.*, **1994**, 33, 4048-4053.
40. S. Aime, M. Botta, G. Ermondi, E. Terreno, P. L. Anelli, F. Fedeli and F. Uggeri, *Inorg. Chem.*, **1996**, 35, 2726-2736.
41. M. P. M. Marques, C. Geraldes, A. D. Sherry, A. E. Merbach, H. Powell, D. Pubanz, S. Aime and M. Botta, *Journal of Alloys and Compounds*, **1995**, 225, 303-307.
42. S. R. Zhang, X. Y. Jiang and A. D. Sherry, *Helvetica Chimica Acta*, **2005**, 88, 923-935.
43. M. R. Spirlet, J. Rebizant, J. F. Desreux and M. F. Loncin, *Inorg. Chem.*, **1984**, 23, 359-363.
44. L. Fusaro, G. Casella and A. Bagno, *Chemistry-a European Journal*, **2015**, 21, 1955-1960.
45. L. Fusaro and M. Luhmer, *Inorg. Chem.*, **2014**, 53, 8717-8722.
46. J. Drader, Understanding and utilizing DOTA coordination chemistry for trivalent lanthanide/actinide separation, Washington State University, 2012.
47. S. Kannengiesser, Optimization of the Synthesis of Ac-225-labelled DOTA-Radioimmunoconjugates for Targeted Alpha Therapy based on Investigations on the Complexation of Trivalent Actinides by DOTA, Ruprecht-Karls-Universität Heidelberg, 2013.

48. M. Audras, L. Berthon, N. Martin, N. Zorz and P. Moisy, *Journal of Radioanalytical and Nuclear Chemistry*, **2015**, 303, 1897-1909.
49. P. Thakur, J. L. Conca and G. R. Choppin, *J. Coord. Chem.*, **2011**, 64, 3215-3237.
50. E. Toth and E. Brucher, *Inorganica Chimica Acta*, **1994**, 221, 165-167.
51. P. Thakur, J. L. Conca, C. J. Dodge, A. J. Francis and G. R. Choppin, *Radiochim. Acta*, **2013**, 101, 221-232.
52. G. X. Tian, Z. Y. Zhang, L. R. Martin and L. F. Rao, *Inorg. Chem.*, **2015**, 54, 1232-1239.
53. J. F. Desreux, E. Merciny and M. F. Loncin, *Inorg. Chem.*, **1981**, 20, 987-991.
54. á. Ravel and M. Newville, *Journal of Synchrotron Radiation*, **2005**, 12, 537-541.
55. N. VanHung and J. J. Rehr, *Phys. Rev. B*, **1997**, 56, 43-46.
56. A. L. Ankudinov, B. Ravel, J. J. Rehr and S. D. Conradson, *Phys. Rev. B*, **1998**, 58, 7565-7576.
57. A. Michalowicz, *EXAFS Code to be found under http://www.icmpe.cnrs.fr/spip.php?article602*.
58. I. Farnan and C. Berthon, *SPR-Nuclear Magnetic Resonance*, Royal Society of Chemistry; Gld edition (May 11, 2016), 2016.
59. X. Y. Cao, M. Dolg and H. Stoll, *Journal of Chemical Physics*, **2003**, 118, 487-496.
60. X. Y. Cao and M. Dolg, *Journal of Molecular Structure-Theochem*, **2002**, 581, 139-147.
61. M. Dolg, H. Stoll and H. Preuss, *Journal of Chemical Physics*, **1989**, 90, 1730-1734.
62. M. Dolg, H. Stoll, A. Savin and H. Preuss, *Theoret. Chim. Acta*, **1989**, 75, 173-194.
63. H. M. Steele, D. Guillaumont and P. Moisy, *Journal of Physical Chemistry A*, **2013**, 117, 4500-4505.
64. T. A. Keith, *AIMALL (aim.tkgristmill.com)*, (2017) TK Gristmill Software, Overland Park KS, USA.
65. C. A. Chang, Y. L. Liu, C. Y. Chen and X. M. Chou, *Inorg. Chem.*, **2001**, 40, 3448-3455.
66. M. Autillo, L. Guerin, H. Bolvin, P. Moisy and C. Berthon, *Physical Chemistry Chemical Physics*, **2016**, 18, 6515-6525.
67. F. H. David and B. Fourest, *New J. Chem.*, **1997**, 21, 167-176.
68. S. Aime, M. Botta and G. Ermondi, *Inorg. Chem.*, **1992**, 31, 4291-4299.
69. S. Aime, M. Botta, M. Fasano, M. P. M. Marques, C. F. G. C. Geraldes, D. Pubanz and A. E. Merbach, *Inorg. Chem.*, **1997**, 36, 2059-2068.
70. D. Lundberg and I. Persson, *Coordination Chemistry Reviews*, **2016**, 318, 131-134.
71. V. S. Bryantsev and B. P. Hay, *Dalton Transactions*, **2015**, 44, 7935-7942.
72. L. E. Roy, N. J. Bridges and L. R. Martin, *Dalton Transactions*, **2013**, 42, 2636-2642.
73. L. Petit, L. Joubert, P. Maldivi and C. Adamo, *J Am Chem Soc*, **2006**, 128, 2190-2191.
74. M. J. Tassell and N. Kaltsoyannis, *Dalton Transactions*, **2010**, 39, 6719-6725.
75. Q.-R. Huang, J. R. Kingham and N. Kaltsoyannis, *Dalton Transactions*, **2015**, 44, 2554-2566.
76. M. B. Jones, A. J. Gaunt, J. C. Gordon, N. Kaltsoyannis, M. P. Neu and B. L. Scott, *Chem Sci*, **2013**, 4, 1189-1203.
77. A. Kerridge, *Dalton Transactions*, **2013**, 42, 16428-16436.
78. A. Kerridge, *Rsc Adv*, **2014**, 4, 12078-12086.
79. R. F. W. Bader, *Chem. Rev.*, **1991**, 91, 893-928.
80. H. Wu, Q. Y. Wu, C. Z. Wang, J. H. Lan, Z. R. Liu, Z. F. Chai and W. Q. Shi, *Dalton Transactions*, **2016**, 45, 8107-8117.

81. Q. R. Huang, J. R. Kingham and N. Kaltsoyannis, *Dalton Transactions*, **2015**, 44, 2554-2566.
82. P. D'Angelo, A. Zitolo, V. Migliorati, G. Chillemi, M. Duvail, P. Vitorge, S. Abadie and R. Spezia, *Inorg. Chem.*, **2011**, 50, 4572-4579.
83. F. H. David and V. Vokhmin, *New Journal of Chemistry*, **2003**, 27, 1627-1632.
84. P. D'Angelo, A. Zitolo, V. Migliorati, G. Chillemi, M. Duvail, P. Vitorge, S. Abadie and R. Spezia, *Inorg. Chem.*, **2011**, 50, 4572-4579.
85. Y. H. Jang, M. Blanco, S. Dasgupta, D. A. Keire, J. E. Shively and W. A. Goddard, *J Am Chem Soc*, **1999**, 121, 6142-6151.